CHAPTER 5

NON-RIGID REGISTRATION (COMPUTED TOMOGRAPHY – ULTRASOUND) OF LIVER USING B-SPLINES AND FREE FORM DEFORMATION

Highlights of the Chapter

- *Two separate algorithms for deformable registration including refinement are explored.*
- *One algo utilizes multilevel B-spline while the other uses gradient information.*
- *Three optimization algorithms are employed and inspected precisely.*

Abstract:

Medical Image registration is a key enabling technology and a highly challenging task. Medical images captured using different modalities (sometimes same modality) undergo the process of registration for applications like the diagnosis of a tumor, image-guided surgery, image-guided radiotherapy, etc. By iteratively minimizing a cost function and optimizing transformation parameters, the registration is achieved. In this paper, the semi-automatic non-rigid registration method is utilized in order to register computed tomography (CT) and ultrasound (US) images of the liver. The global motion is modeled by an affine transformation, while the local motion is described by Free Form Deformation (FFD) based on B-Splines. As the existence of local deformation between US and CT images is inevitable due to respiratory phases, two different techniques are included and investigated for registration refinement: transformation using Multi-level B-splines and using gradient orientation information. This work also includes and inspects three different types of optimization strategies: Steepest Gradient Descent, quasi-Newton and Levenberg-Marquardt method. This method is tested on six clinical datasets, and

quantitative measures are assessed. Visual examinations and experimental results verify a lower level of registration error and a higher degree of accuracy when the method is employed using Levenberg-Marquardt optimization utilizing gradient orientation information for registration refinement.

5.1. Introduction

Defining a spatial transformation (or mapping) which correlates the features or anatomical points of one image to corresponding positions of another image is the basic idea of image registration. The notion of correspondence varies depending on the application. Applications can be oriented towards structural correspondence (aligning the same anatomical structures) or functional correspondence (aligning functionally equivalent regions) or structural-functional both. Registration can be described as integration of three components [7]:

- A similarity measure which describes the level of match between images (source and target).
- A transformation model which transforms the source image in order to match it with the target image (up-gradation of transformation parameters upgrades the transformation model).
- An optimization process which iteratively helps in upgrading the transformation parameters by maximizing the similarity measure (or by minimizing the cost function).

A registration algorithm (rigid and non-rigid) adds values to images by providing a single coordinate system to the structural (CT, MRI, US) and functional (PET, SPECT, fMRI) images for viewing and analysis.

Various imaging modalities (CT, MRI, PET, US, SPECT, etc.) are widely used these days not only by doctors and physicians for clinical diagnosis but also by researchers for comprehensive studies, screenings and most prominently for up-gradation of the imaging and image processing techniques. These modalities provide output in form of an image with a large

amount of detailed data which greatly helps in medical image analysis. One of the most popular imaging systems is Ultrasound (US) as it is less expensive, it does not use X-rays, the imaging is non-invasive, and the output shows up in real-time. For the abdominal portion (specifically for liver), US scanners are extensively used in intervention procedures as a guidance tool in ethanol injection therapy, percutaneous needle biopsy, high intensity focused ultrasound therapy (HIFU), radiofrequency ablation (RFA), etc.

5.1.1. Background

Clinicians often face problems to clearly identify a target lesion as US images have relatively lower image quality than CT or MR image. To overcome this limitation, various researches have been carried out to register US image to its corresponding CT/MR image to provide correct and clear details about the lesions or the anatomy of the organ. The output of the registration with sufficient accuracy delivers detailed information which helps surgeons and radiologists in treatment planning. Since the liver undergoes respiratory (involuntary) motion, the captured image includes local non- rigid deformations which are not always possible to compensate with rigid registration algorithms. Hence, to achieve precise alignment of US and CT images, non-rigid registration is definitely required. For multimodality image registration, the biggest issue is the contrast of the images, which differs most of the time. The characteristics of US image differs from CT image which leads to intensity mismatch for any particular region which makes the estimation of the relationship between corresponding pixels complex. The relationship is very crucial to determine an objective function which is defined as the similarity/ dissimilarity measure and necessary for a successful registration.

Development of semi-automatic method for non-rigid registration of CT and US images is described in this paper. The distinguished advantage of the process is that the information theory-based similarity measure mutual information is combined with the non-rigid transformation model of the liver. Three different optimization strategies (Steepest Gradient Descent, quasi-Newton and Levenberg-Marquardt method) are employed and evaluated separately with respect to accuracy and precision for the complete registration process.

5.1.2. Related Work

The fact that the liver is subjected to respiratory motion and its degree of movement varies with the patient is demonstrated in [31]. [28] describes that the deformation in the liver image caused by this motion can be compensated using non-rigid registration. Also, during US scanning, the probe pressure can cause local deformation to the abdominal organs [33, 20]. The abdominal organ motion during respiration is measured in [3]. To register the US and CT image, [25] has utilized a voxel-based approach where normalized cross-correlation is used as a similarity measure to optimize the rigid transformation parameters but, before that, the image intensities are remapped, and images are converted into vessel probability images. The same kind of approach is presented in [34] where a semi-affine transformation model is used for registration with correlation ratio taken as a similarity measure after generating a simulated US image from the CT image. [26] proposed a feature-based approach, to utilize the vessel centerline and liver surface as features. A manual segmentation step is required for that. In this approach, the objective function is the average closest distance between corresponding features and an ICP based registration algorithm is developed. As the relationship between CT and US images varies with organs, an organ independent objective function is developed by [39]. [27]

introduce a US-MR image registration technique where the similarity measure is a bivariate correlation ratio calculated by correlating both the intensity and the gradient magnitude. A US-CT image registration algorithm of the spine is proposed by [4] where the average intensity value of the corresponding points is taken as the objective function. [5] adopted mutual information as a similarity measure for the registration of US and CT prostate images. Considering local deformations, a non-rigid registration algorithm defining the spatial relationship using FFD and B-Splines is developed in [29] and employed on breast MR images. B-Splines are also used in [38] to precisely model the non-rigid transformation. Additional Power Doppler (PD) is utilized in [14] to develop an ICP based image registration algorithm using the information of vessel centerlines for registering US and CT images. [9] estimated the transformation between PD US and CT images by defining an energy function based on the prior information about landmarks and normalized gradient fields. Parametric transformation is developed using B-Splines and FFD for CT and US images of liver and the similarity measure is based on the intensity and gradient information [16]. Landmark-intensity combined information is utilized in [15]. A non-rigid registration technique is developed in [19] for High-Intensity Focused Ultrasound (HIFU) system. [34] extended their work in [35] by modifying the similarity measure based on local cross-correlation to obtain a precise deformable registration. Transformation technique based on robust edge matching is developed in [21]. In [36, 37] they again extended their algorithm for position estimation of moving liver and feature-based pre-registration of US and MR images.

This paper is organized as follows. In Section 5.2, the entire image registration method combining the global and local model, similarity measure and regularization method are

described. The following section is dedicated to registration refinement which includes the detailed procedure of multilevel B-Splines and formation of gradient orientation based objective function. Section 5.4 includes the details of the optimization methods. Section 5.5 consists of experiments with clinical datasets, experimental results and discussion. Finally, in Section 5.6 conclusions are drawn.

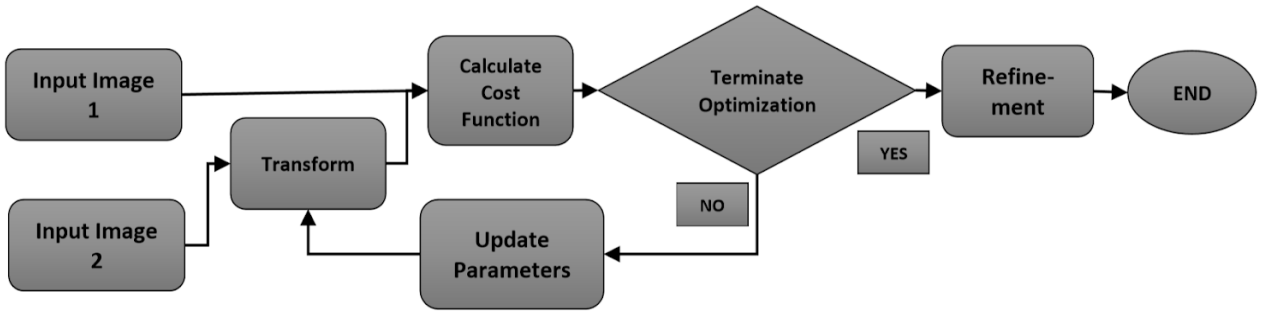

Fig. 5.1. Block diagram of image registration

5.2. Methodology (Image Registration)

The basic structure of the proposed method is shown in Fig. 5.1. The objective of the image registration algorithm is to map selected regions or points in the CT image on the corresponding points in the US image. The procedure mainly involves a search process for the optimal transformation. Finding out a parametric transformation T is the goal of the proposed algorithm that precisely aligns the moving US image to the fixed CT image by minimizing a cost function through an optimization procedure. Considering the non-rigid motion of the liver and the poor quality of ultrasound images, the semi-automatic registration algorithm is developed combining a global affine transformation and a local non-rigid transformation.

$$T(x, y) = T_{global}(x, y) + T_{local}(x, y) \tag{5.1}$$

5.2.1. Preprocessing

A preprocessing step is required for both US and CT images. As US image suffers from speckle noise, a suitable denoising filter using variation minimization is applied for removing noise while preserving the edges. CT image does not contain that much of noise, but the images are filtered, preserving the low contrast edges, in order to improve the contrast of the same. Hence, a contrast enhancement procedure is utilized to get a better output.

5.2.2. Global Motion Model

The overall motion of the liver is described by the global motion model. To represent the whole region of interest, a general class of affine transformation [8] model is utilized which is parameterized in 6 degrees of freedom describing the translation, rotation, scaling and shearing by the coefficients Θ. In 2D, affine transformation can be represented as follows:

$$T_{global}(x, y) = \begin{bmatrix} x' \\ y' \end{bmatrix} = \begin{bmatrix} a_0 & a_1 \\ b_0 & b_1 \end{bmatrix} \begin{bmatrix} x \\ y \end{bmatrix} + \begin{bmatrix} a_2 \\ b_2 \end{bmatrix} \tag{5.2}$$

As US image is of poor quality and low signal-to-noise ratio, control point pairs from both US and CT images are selected manually to compute the parameters of the affine transformation model in order to ensure the accuracy of the registration process.

5.2.3. Local Motion Model

After capturing the global motion of the liver by affine transformation, the local deformation is still present, and an additional non-linear transformation is required to model that. A Free Form Deformation (FFD) model [6,10,30] based on B-Splines, which is very useful to model 3D deformable objects, is applied to this algorithm for modelling the local deformation of the liver. For m_x, m_y being the size of the moving image, the number of control points is:

$$n_x = \lceil \frac{m_x}{\delta_x} \rceil + 3 \; ; \; n_y = \lceil \frac{m_y}{\delta_y} \rceil + 3 \tag{5.3}$$

The non-rigid transformation $T_{local}(x, y)$ is defined on a uniformly spaced grid Φ $(n_x \times n_y)$ of control points $\varphi_{i,j}$ where $[-1 \leq i < n_x\text{-}1$ and $-1 \leq j < n_y\text{-}1]$ with uniform spacing of δ_x and δ_y in the x and y direction respectively. For any pixel location (x, y), the FFD is calculated from the surrounding 4×4 control points.

$$T_{local}(x, y) = \sum_{l=0}^{3} \sum_{m=0}^{3} B_l(u) B_m(v) \varphi_{i+l,j+m} \tag{5.4}$$

The index of the control point cell containing the pixel (x, y) is denoted by i, j, while the relative position is defined by u, v. Using control point grid spacing δ_x and δ_y, these can be defined as:

$$i = \lfloor \frac{x}{\delta_x} \rfloor - 1 \; ; \; y = \lfloor \frac{y}{\delta_y} \rfloor - 1 \tag{5.5}$$

$$u = \frac{x}{\delta_x} - (i + 1) \; ; \; v = \frac{y}{\delta_y} - (j + 1) \tag{5.6}$$

The basis functions B_0 to B_3 are the third order spline polynomials and can be defined as:

$$B_0(t) = (-t^3 + 3t^2 - 3t + 1)/6 \tag{5.7}$$

$$B_1(t) = (3t^3 - 6t^2 + 4)/6$$

$$B_2(t) = (-3t^3 + 3t^2 + 3t + 1)/6$$

$$B_3(t) = t^3/6$$

As the B-Splines are locally controlled, using this for a large number of control points is computationally efficient. The coordinate transformation is defined by $(x, y) \rightarrow (x, y) + T_{local}(x, y)$. Changing the position of a control point affects only the neighborhood of that point. This implies that basis functions of cubic B-Splines have limited support.

5.2.4. Similarity Measure

A similarity criterion must be defined to measure the level of alignment while registering the moving US image ($I_{m_{US}}$) with the fixed CT image ($I_{m_{CT}}$). The similarity measure should have a local or global maximum if the two images are correctly aligned. While calculating a statistical relationship between two multimodality images, information theoretic similarity measure Mutual Information (MI) has shown

very accurate and robust output. The calculation does not require any landmark or surface to be pointed out. Instead it uses only image intensities and thus not limited to segmentation errors. Mutual Information was first proposed in [6] and is provides the amount of information that one image $I_{m_{CT}}$ contains about the second image $I_{m_{US}}$ [18].

$$MI\left(I_{m_{CT}}, I_{m_{US}}\right) = H\left(I_{m_{CT}}\right) + H\left(I_{m_{US}}\right) - H\left(I_{m_{CT}}, I_{m_{US}}\right) \tag{5.8}$$

Where $H\left(I_{m_{CT}}\right)$ & $H\left(I_{m_{US}}\right)$ are the marginal entropies and $H\left(I_{m_{CT}}, I_{m_{US}}\right)$ is the joint entropy of both images, calculated from the 2D joint histogram of corresponding pixel values in the overlap region of $I_{m_{CT}}$ & $I_{m_{US}}$ .Mutual information is maximized when both images are aligned. To overcome the dependency of MI on the image overlap, [32] suggested to use the normalized mutual information (NMI) as a measure of alignment.

$$NMI\left(I_{m_{CT}}, I_{m_{US}}\right) = \frac{H\left(I_{m_{CT}}\right) + H\left(I_{m_{US}}\right)}{H\left(I_{m_{CT}}, I_{m_{US}}\right)} \tag{5.9}$$

5.2.5. Deformation Regularization

All types of deformations are not physically plausible. A local deformation should be characterized by a smooth transformation. A displacement field created by the deformations is

considered to be smooth if the magnitude and the direction of displacements change gradually in its neighborhood with no harsh jumps. Therefore registration algorithms are often regulated using a special technique which evaluates the deformation and penalizes it if it is considered irregular. To constrain the B-Spline based FFD transformation to be smooth, a penalty term is introduced in the cost function which defines the bending energy of a thin plate of metal.

$$C_{reg} = \int_0^X \int_0^Y \left[\left(\frac{\partial^2 T}{\partial x^2} \right)^2 + \left(\frac{\partial^2 T}{\partial y^2} \right)^2 + 2 \left(\frac{\partial^2 T}{\partial x \partial y} \right)^2 \right] dx\, dy \tag{5.10}$$

5.2.6. Optimization

To find the optimal transformation by calculating the deformation parameters, a cost function associated with the global and local transformation is minimized through an optimization process. It consists of two terms. The first term describes the level of similarity between images, where the second term corresponds to the smoothness of the transformation.

$$C_f = -NMI + \lambda C_{reg} \tag{5.11}$$

Here λ is a weighted coefficient which defines the tradeoff between the similarity measure and the smoothness of the transformation. Three different optimization strategies are employed and tested separately for calculating the non-rigid transformation parameters: Steepest Gradient Descent, quasi-Newton and Levenberg-Marquardt method.

5.3. Registration Refinement

Although using the abovementioned transformation model, we get the transformation parameters for registering the US and CT image, but its level of accuracy is not that much satisfactory. To improve the registration accuracy, refinement is a necessary step. Two different procedures are tested for this

purpose. The first method is a multi-resolution approach where B-Spline control grid resolution is increased in a coarse to fine fashion. The second method utilizes the liver surface properties and gradient orientation information as additional information to refine the registration result.

5.3.1. Using Multi-level B-splines

The basic idea behind this approach is to model deformations on various resolutions of B-Spline control point grid [17]. If the control points are very close, they are sensitive enough to capture small deformations, while large deformations are tough to reconstruct precisely since a lot of control points have to move over large distances. Similarly, a coarse control point grid is unable to capture deformations which are smaller than control point distance, but global deformations can be modeled effectively. So the non-rigid registration algorithm (transformation T_{local} estimation) is divided into multi levels on the basis of control point grid resolution in order to combine the advantage of both coarse and fine grid.

Let the hierarchy of the control point grid at different resolutions is denoted by $\Phi_1, \ldots, \Phi_k$. The initial registration starts with the coarse grid. The grid resolution increases from Φ_{k-1} to Φ_k and spacing between the control points decreases. The transformed control points position φ_i' can be calculated from its previous coarse control points φ_i.

$$\varphi'_{2i+1} = \tfrac{1}{2}(\varphi_i + \varphi_{i+1}) \tag{5.12}$$

$$\varphi'_{2i} = \tfrac{1}{8}(\varphi_{i-1} + \varphi_{i+1} + 6\varphi_i) \tag{5.13}$$

After registration at a particular coarse grid level, the control point configuration reflects the deformation captured at that level. The new grid of the next finer resolution level with twice as many control points is constructed from the old one by inserting a new control point between

every pair on the coarse grid. Using above-mentioned equations, a finer control grid with twice the resolution is obtained with same displacement field as of the previous coarse grid (Fig. 5.2).

Algorithm-1 (affine + multilevel B-Spline)

---

calculate the affine transformation parameters
initialize the control points
repeat
    calculate the value of cost function using equation (5.11)
    while not reached convergence
        update the position of control points
        recalculate the value of cost function using equation (5.11)
    increase the control point grid resolution using equation (5.12) and (5.13)
until the final level of control point grid resolution or convergence is reached.

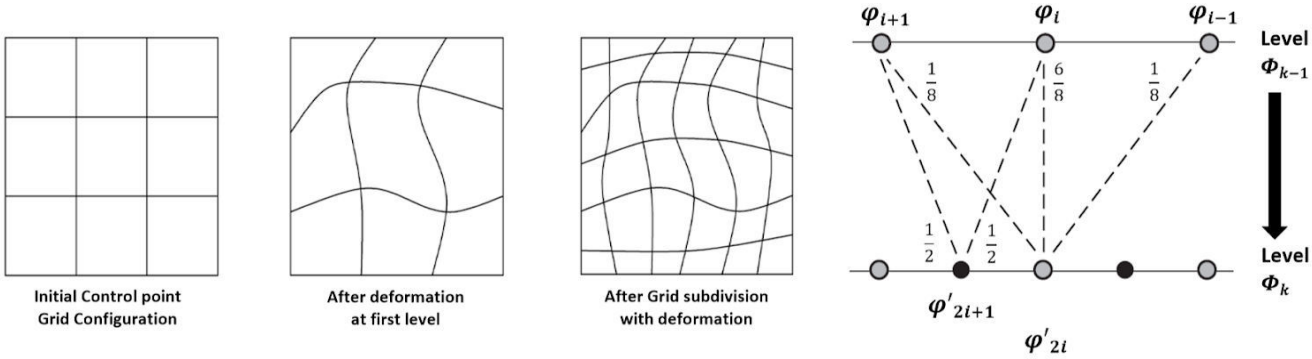

Fig. 5.2. Configuration of multi-resolution control point grid;
Refinement of grid with deformation (left); Calculation of grid subdivision (right)

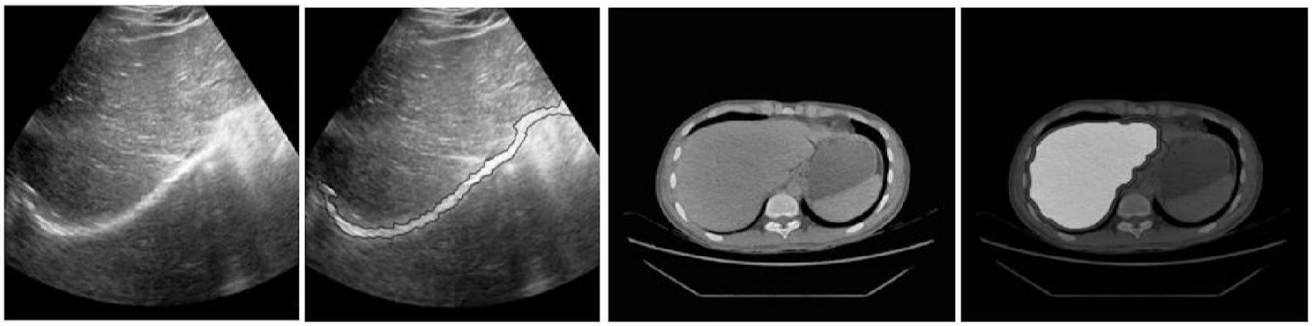

Fig. 5.3. US image (leftmost); US image with masking (second from left); Enhanced CT image (third from left); Enhanced CT image with masking (rightmost); Image reproduced from [2]

5.3.2. Using Gradient Orientation Information

Once the preliminary registration (affine & non-rigid) of the CT and US image is completed, the result is refined using another non-rigid registration of those CT and US liver surface masked images, by minimizing an objective function based on the pixel intensity and gradient orientation information [13]. The detailed algorithm is as follows.

5.3.2.1. Segmentation (Mask Generation)

The liver surface feature is very useful for the step of registration refinement. In US images, the diaphragm or the liver surface boundary produces high intensity values. While in CT images, almost similar intensity can be seen in liver surface regions. So one step image enhancement helps CT images in producing high gradient values in the boundary of the liver surface area. An automatic segmentation procedure [1] is implemented to track the liver surface boundary and to produce mask images. Isolating the largest connected component in the selected region of interest (ROI) is the basic idea for liver segmentation in CT images. Tracking the connected pixels with high intensity values using morphological operations helped in segmenting liver surface after a successful adaptive binarization of US images. The mask images contain the pixels within the liver surface boundary region only. Thus the liver surface masked images of CT and US are developed for further computation (shown in Fig. 5.3).

5.3.2.2. Entropy Based Objective Function

It is likely that the liver surface boundary or edge region of both masked US and CT images will be aligned and their edge orientations will be the same when two images are perfectly registered. So, an edge orientation coincidence function E_{OC} can be defined as,

$$E_{OC}(\Delta\theta) = \tfrac{1}{2}(1 + cos\ (2\Delta\theta)\ ) \tag{5.14}$$

Where $\Delta\theta$ represents the gradient orientation angle difference between pixels of CT and US image. Now a 3D joint histogram is constructed using the corresponding pixel intensities along with the E_{OC}. Edge orientation coincidence is reflected here as local spatial information which is combined with the statistical information of the pixel intensity values in order to define an entropy based objective function. Since gradient magnitude values are more prominent than pixel intensity at the liver surface edges of the CT images, $|\nabla I_{m_{CT}}|$ is used instead of using direct intensity values. The function is specified as a sum of three conditional entropies.

$$\begin{aligned} E\left(|\nabla I_{m_{CT}}|, I_{m_{US}}\right) &= H\left(|\nabla I_{m_{CT}}|\,|\,I_{m_{US}}\right) + H\left(|\nabla I_{m_{CT}}|\,|\,I_{m_{CT}}\right) + H\left(E_{OC}|\,|\nabla I_{m_{CT}}|, I_{m_{US}}\right) \\ &= H\left(|\nabla I_{m_{CT}}|, I_{m_{US}}, E_{OC}\right) - \left[H\left(|\nabla I_{m_{CT}}|\right) + H\left(I_{m_{US}}\right) - H\left(|\nabla I_{m_{CT}}|, I_{m_{US}}\right)\right] \\ &= H\left(|\nabla I_{m_{CT}}|, I_{m_{US}}, E_{OC}\right) - M\left(|\nabla I_{m_{CT}}|, I_{m_{US}}\right) \end{aligned} \tag{5.15}$$

Here $M\left(I_{m_{CT}}, I_{m_{US}}\right)$ is the mutual information. The entropy based function $E\left(I_{m_{CT}}, I_{m_{US}}\right)$ is calculated only for the overlapping regions of mask images. As the entropy term contains local spatial information, partial overlapping can cause the false global minimum problem which leads to wrong registration. To alleviate the problem, a global spatial function is introduced.

$$F\left(I_{m_{CT}}, I_{m_{US}}\right) = \left(1 - C\left(I_{m_{CT}}, I_{m_{US}}\right)\right).\left(E\left(|\nabla I_{m_{CT}}|, I_{m_{US}}\right)\right) \tag{5.16}$$

where,
$$C\left(I_{m_{CT}}, I_{m_{US}}\right) = (N_{CT} + N_{US})^{-1}.\left(\sum_{p\in(R_{CT}\cap R_{US})}\left(1 + cos\left(\Delta\varphi_p\right)\right)\right) \tag{5.17}$$

so,
$$F_c\left(I_{m_{CT}}, I_{m_{US}}\right) = F\left(I_{m_{CT}}, I_{m_{US}}\right) + \lambda C_{reg} \tag{5.18}$$

F_c is the objective function including regularization C_{reg}. R_{CT} and R_{US} define the edge regions of masked CT and US images respectively. Similarly, N_{CT} and N_{US} denote the number of pixels in the regions R_{CT} and R_{US}.

5.3.2.3. Transformation Estimation

Again FFD with B-Splines is adopted for this pixel based registration using same level control point distribution as previous while minimizing the newly constructed objective function containing local & global spatial information with MI (including the regularization term).

$$\dot{t_p} = arg\ min_{t_p}\ F_c\left(I_{m_{CT}}, I_{m_{US}}\ ; t_p\right) \tag{5.19}$$

Transformation parameters are the position of control points which will provide the best registration refinement at their optimal positions. Here also three different optimization techniques are tested to compute the best values of transformation parameters.

Algorithm-2 (affine + non-rigid_1_using MI + non-rigid_2_using Gradient orientation info)

calculate the affine transformation parameters
calculate the value of cost function using equation (5.11)
while not reached at convergence
    update the position of control points
    recalculate the value of cost function using equation (5.11)
segment the CT and US image
generate the Mask images
initialize the control points again
calculate the value of cost function using equation (5.18)
while not reached convergence
    update the position of control points
    recalculate the value of cost function using equation (5.18)

5.4. Optimization

5.4.1. Steepest Gradient Descent Method

During optimization, to incorporate the gradient information in the minimization process of the function, steepest gradient descent is the best and most straightforward method [12] for that. The minimum value of the function is found by reiterating the 1D line minimization step for

several times. Considering a simple problem of minimization of a function $f(x)$ in 1D space. An initial value of the function is x_0. So the minimum of the function can be found iteratively by,

$$x_{n+1} = x_n - \alpha f'(x_n) \tag{5.20}$$

Here $f'(x_n) = \frac{d}{dx} f(x) = \nabla f(x)$ is the derivative of the function and $\alpha > 0$ is the positive parameter which controls the step size. The updated solution x_{n+1} is found to be improved when the value of $f(x_{n+1})$ is smaller than the value of $f(x_n)$. When a point is found where $f'(x_n) = 0$, it implies that the minimum of the function (can be local or global) has been reached. Each step starts from the minimum found in the previous step and it proceeds towards the direction of the gradient of that point. But steepest gradient descent cannot be considered as a very good algorithm. The optimum value of the function is not necessarily pointed by the gradient. Also the consecutive steps are strictly at orthogonal angles towards the optimum. So while going downwards to a long and narrow valley, a lot of tiny steps are required to reach the optimum.

5.4.2. Quasi-Newton Method

Newton-Raphson algorithm is the original inspiration behind the idea of the quasi-Newton optimization method. Second order information is used while optimizing a function $f(x)$ and this property gives the algorithm a better convergence than gradient descent. The minimization is implemented using,

$$x_{n+1} = x_n - \alpha \ [H(x_n)]^{-1} f'(x_n) \tag{5.21}$$

Here, $H(x_n)$ denotes the Hessian matrix of the cost function which is evaluated at x_n and α is the gain factor which confirms the progress of the optimization. The gain factor α is determined

by combining the quasi-Newton method with an inexact line search routine. The computation of Hessian matrix and its inverse is computationally very expensive, particularly for non-rigid registrations which are high dimensional optimization problems. At this point, quasi-Newton algorithm tackles the problem by iteratively building up a good approximation of the inverse Hessian matrix $[H(x_n)]^{-1}$. Thus, the need of a matrix inversion is avoided by direct approximation of inverse Hessian. The first approximation of the inverse Hessian is taken as the identity matrix. In each iteration n, the approximation is updated. The update does not require the second order derivatives of the cost function, only first order derivatives are enough for this computation. A few notable approaches to iteratively update inverse Hessian are Davidon-Fletcher-Powell (DFP), Symmetric_Rank-1 (SR1) and Broyden-Fletcher-Goldfarb-Shanno (BFGS). BFGS is proven to be very efficient in various numerical experiments [23]. The limited memory BFGS (LBFGS) optimizer which is a popular variant of BFGS is utilized in this paper.

5.4.3. Levenberg-Marquardt method

Minimization problems are very similar to the least-squares problems. The basic idea behind least-square problems for a function $f(x)$ of N dimensions is to recover the N parameters x^* for which the least-squares figure of merit $f^2(x^*)$ is minimum. Levenberg and Marquardt have provided a method for general non-linear least squares. This method calculates the incremental update Δx_n from the current estimate x_n. By this step, the method smoothly varies between the inverse Hessian matrix approach and the steepest Gradient Descent approach. The equation which is utilized for this method is given below.

$$(H_n + \omega I) \,.\, \Delta x_n = -\nabla f^2 = -2f \,.\, \nabla f \tag{5.22}$$

Here H_n is the Hessian of f^2 at x_n, the parameter ω defines the regularization and I is the identity matrix. If f^2 is quadratic, then the equation converts to the process of inverse Hessian method,the $H_n \,.\, \Delta x_n = -\nabla f^2$. This happens when the parameter ω approaches to zero and the equation directly goes to the optimum from x_n. For a larger value of ω, the equation converts to $\Delta x_n \approx -\nabla f^2$, as $(H_n + \omega I)$ becomes diagonally dominant, becoming steepest descent approach.

The Hessian matrix is estimated by using only the first derivative terms and ignoring the second derivative terms. Using a moderate value of ω, Δx_n is calculated from the equation and f^2 is evaluated at $x_n + \Delta x_n$. Now, if $f^2(x_n + \Delta x_n) \geq f^2(x_n)$, the value of ω is increased, the method approaches towards the steepest descent with Δx_n taken as the new step. If $f^2(x_n + \Delta x_n) < f^2(x_n)$, the method shift towards the inverse Hessian by decreasing the ω, and $x_{n+1} = x_n + \Delta x_n$ is taken as the new estimate for optimum. When f^2 decreases by a very small amount, it is assumed to be reached at convergence. A lot of function evaluation can be avoided by using this optimization method as no line minimization is performed at each iteration.

5.5. Experimentation

5.5.1. Data Acquisition

For performance evaluation of the algorithm, six datasets are taken into account. Each dataset consists of the CT and US image data of the patient's abdominal region. The CT images (dimension 512 × 512) are acquired using a 64 slice CT scanner machine (multi-detector row scanner, 64 rows of detector) of GE medical Health Systems. A 3.5 MHz trans-abdominal electronic array transducer of an Ultrasonography machine of Philips Medical System is used to capture the B-mode US images (dimension 1024 × 768). 20 images of 2D US and 10 CT images

are used to construct one dataset. 10 of the US images of one dataset is taken in the axial plane, and the remaining 10 images are captured in the sagittal plane. The 2D CT images are captured in the axial plane. The CT and US images are acquired at the end-inspiration of the respiratory phase with a breath hold. Both CT and US images captured are cropped then and converted to a fixed dimension before further computation. The coarse grid of multilevel B-Spline control point structure is defined using 8 × 8 mesh of control points while the finest level is a 32 × 32 mesh of control points. Another non-rigid transformation with gradient orientation information is utilized using a 32 × 32 mesh. The weighted coefficient λ is set to 50 for the calculation of all datasets.

5.5.2. Experimental Results

The CT-US image registration results are shown in Fig. 5.5. For a simple registration accuracy assessment by visualizing the images, the registered images of both the algorithms (with every optimization technique) are provided. The three columns are designated to the three different types of optimization techniques. The first column specifies the registration with Steepest Gradient Descent (SGD) method, quasi-Newton (QSN) method and Levenberg-Marquardt (LVM) method respectively. Similarly, row-wise, in the first and second row, only the US and CT images are shown. Third row specifies the results of Algorithm-1 (affine + multilevel B-Spline) followed by the registration Algorithm-2 (affine + non-rigid_1_using MI + non-rigid_2_using Gradient orientation information) at the fourth row. A distance based measure is adopted to evaluate the registration algorithms quantitatively. The distance measure is based on the anatomical feature points segmented from the pairs of US and CT images. The measure can be defined as follows:

$$D_{CT\_US} = 2.(N_A + N_B)^{-1} \sum_{p_{US} \in B} min_{p_{CT} \in A} \{d(p_{CT},\ T(p_{US}))\} \quad (5.23)$$

The extracted feature points of CT and US images are stored respectively as two sets denoted by A and B. Correspondingly, the number of samples in A and B are N_A *and* N_B. The distance between the two feature points is denoted by $d(.)$ which is calculated using the mathematics of Euclidean distance. Feature points of set A for the CT image is taken by using a manual segmentation method, while for set B, a feature extraction algorithm from [11] is employed.

Table 5.1. Registration accuracy test values (Distance Measurement (in mm): Mean (± SD))

Clinical Data	Affine	Algorithm-1			Algorithm-2		
		SGD	QSN	LVM	SGD	QSN	LVM
Dataset 1	4.28 (0.93)	1.78 (0.29)	1.79 (0.33)	1.76 (0.16)	1.7 (0.39)	1.63 (0.27)	1.61 (0.19)
Dataset 2	3.95 (0.88)	1.38 (0.5)	1.32 (0.41)	1.29 (0.08)	1.2 (0.43)	1.21 (0.2)	1.17 (0.32)
Dataset 3	4.5 (0.64)	2.01 (0.33)	1.97 (0.28)	1.99 (0.19)	1.99 (0.24)	1.93 (0.3)	1.95 (0.17)
Dataset 4	4.7 (0.9)	1.8 (0.46)	1.76 (0.22)	1.77 (0.24)	1.93 (0.37)	1.87 (0.25)	1.89 (0.29)
Dataset 5	4.36 (0.56)	1.22 (0.16)	1.08 (0.13)	1.08 (0.21)	1.17 (0.19)	1.01 (0.2)	0.99 (0.22)
Dataset 6	5.22 (0.69)	2.1 (0.37)	1.9 (0.29)	2 (0.15)	1.9 (0.13)	1.87 (0.23)	1.83 (0.31)

5.5.2.1. Accuracy

Table 5.1 and Figure 5.4 shows the mean and standard deviation values of the distance based measure DCT_US for each dataset after registration of images. In the table, D_{CT_US} is provided after registration is done with affine transformation, with Algorithm-1 and with Algorithm-2. It is found that for each algorithm (except affine), the average estimated value of D_{CT_US} is less than 2.5mm. For clinical applications, error of less than 5mm is considered acceptable [24]. This implies that both of the algorithms are good enough in improving the registration accuracy as well as clinically applicable too.

5.5.2.2. Precision (of Optimization Techniques)

In total, 120 registration experiments (20 US-CT registrations per dataset) are done using each of the optimization techniques for each algorithm. To evaluate the precision of optimization techniques, Algorithm 1 and 2 are taken in account separately. The variation of the optimum values calculated by each optimization technique for a single dataset is evaluated by comparing every registration parameter μ with the parameters found for the best optimization result $\mu*$. The Euclidean norm $|\Delta\mu|= |\mu-\mu*|$ of the difference vectors is taken as the base for the comparison of parameter vectors. Table 5.2 shows the values for mean $|\Delta\mu|$ and max $|\Delta\mu|$ for all clinical datasets. The results signifies that Levenberg-Marquardt method is more precise on an average for both the algorithms. Although the maximum values for Algorithm-2 are approximately similar, which infers that their worst case precision are almost the same.

Table 5.2. Precision test results of optimization techniques

	Algorithm 1			Algorithm 2		
	SGD	**QSN**	**LVM**	**SGD**	**QSN**	**LVM**
Mean $\|\Delta\mu\|$	0.087	0.082	0.073	0.075	0.074	0.067
Max $\|\Delta\mu\|$	0.151	0.153	0.15	0.147	0.134	0.141

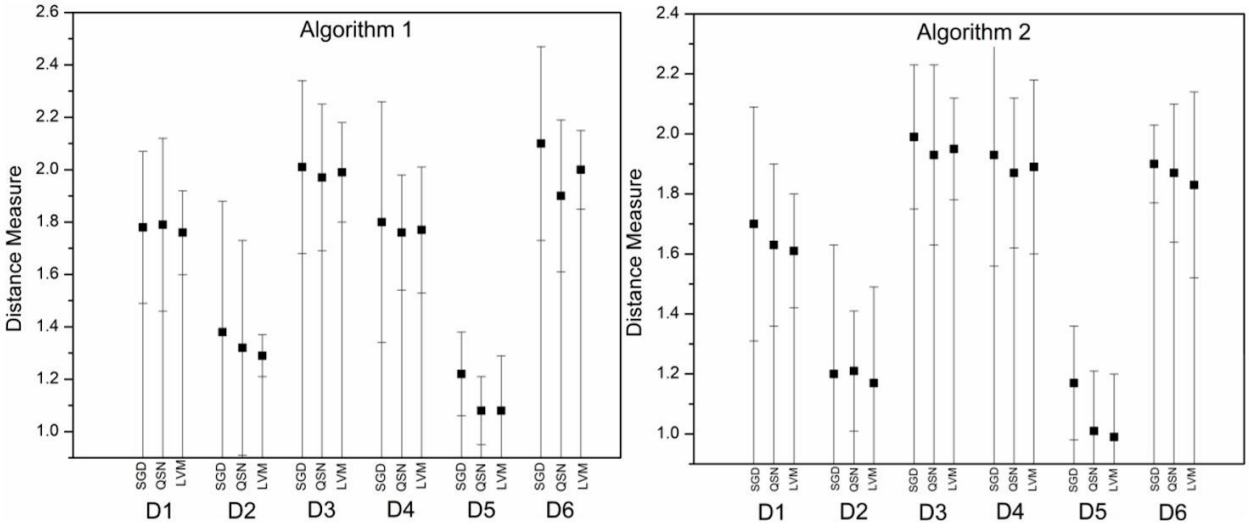

Fig. 5.4. Graphical representation of Distance Measurement values (in mm) for clinical datasets

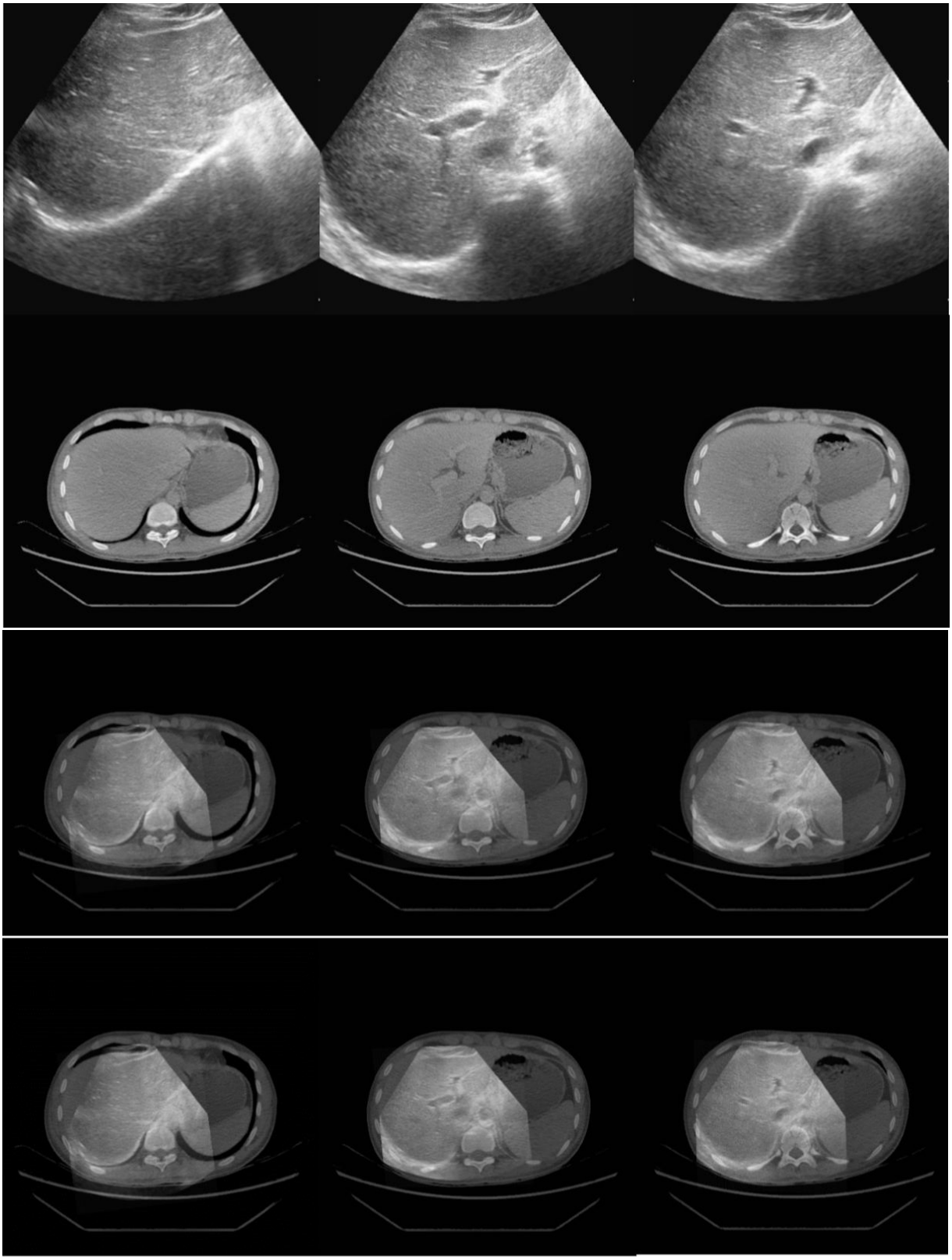

Fig. 5.5. Registration results (Algo-1 & Algo-2, Third & Fourth rows) using SGD (Left); QSN (Middle) and LVM (Right)

5.5.2.3. Discussion

The best method for testing the performance of a registration algorithm is to employ it for the registration of naturally deformed images. Simulated images do not contain any speckle decorrelation, deformation with respiration or motion ambiguities. So testing on the clinical dataset is the best choice left. In this proposed algorithm, at first, some control point pairs are selected to calculate the parameter matrix of affine transformation. Non-rigid registration (with registration refinement) is then performed using two different algorithms. The accuracy is evaluated for both the semi-automatic registration algorithms for CT and US images of the liver. Though the images are taken with breath-hold condition, deformation is positively added to the images automatically for various reasons (internal organ motions, motion of beating heart, etc.). The assumption is proved when the distance measure is calculated just after the affine transform. Values clearly indicate that deformation cannot be modeled by affine transformation only. After the images are registered using non-rigid registration algorithms, the distance measure values of surface regions decrease significantly. It is observed from Table 5.1 that when utilizing Algorithm-2 (affine + non- rigid_1_using MI + non-rigid_2_using Gradient orientation information), almost all (except a few) distance measure values are lesser than the values generated by employing Algorithm-1 (affine + multilevel B- Spline). This implies that Algorithm-2 has better accuracy than Algorithm-1. Also, while carefully observing Table 5.1, it is found that for each dataset, variation of distance measure for varying optimization techniques is very nominal. This indicates that each of these registration converged to the same optimum (almost). From this, it can be inferred precisely that distance measure is independent of the optimization technique.

Although experiments regarding computational efficiency are not included in this paper, it can be easily projected that the computational efficiency of optimization methods is dependent on the computation time of its iterations. Also for the registration algorithms, control point grid resolution is another criterion of computational complexity. Thus the cost function, its derivatives, and grid resolution altogether dominate the computation time per iteration. It is observed from the experiments that Algorithm-1 with Levenberg-Marquardt optimization can provide an output reliable enough in a shorter time (applicable for image guided surgery system) than Algorithm-2 with the same optimization, which provides output with better accuracy and precision at the price of larger computation time (applicable for accurate treatment planning).

5.5.2.4. Limitations

As discussed previously, speed-up of the registration process can be gained by stopping the optimization at lower grid resolution when convergence is reached (for Algorithm-1) or by not using a higher resolution control point mesh (for Algorithm-2). But this will decrease the precision of the optimization methods. Here, the existing trade-off between the computational efficiency and registration model flexibility is a matter of choice which depends on the requirement of accuracy for modeling the deformation. Also, the registration process always relies on the optimization of a parameter space which is prone to getting stuck in local optima, resulting in a large mismatch. This problem can be avoided by carefully choosing the hyperparameters. Lastly, the quality of the medical images are also a matter of concern. As the ultrasound images are of poor quality, the more research should be done on incorporating spatial information and specific intensity models into similarity criterion for improving the accuracy of the registration.

5.6. Conclusion

Development of semi-automatic non-rigid registration algorithm to register CT and US liver images is the basic idea of the paper. Combining global (affine) and local transformation (B-Spline FFD) provides a great flexibility for liver deformation modeling. Results show that both “multilevel B-splines” and “gradient orientation with intensity information” are able to model the deformation precisely (later is slightly better than former). Quantitative evaluations show, that the accuracy is not dependent on any of the optimization procedures (Steepest Gradient Descent, quasi-Newton and Levenberg-Marquardt method) tested, whereas Levenberg-Marquardt optimization is found to be more precise and suitable.

References

1. Bhattacharjee, R. and Saini, L.M. (2015) Robust technique for the detection of acute lymphoblastic leukemia in 2015 IEEE Power, Communication and Information Technology Conference (PCITC), IEEE, pp. 657-662.
2. Bhattacharjee, R., Verma, A., Sharma, N. and Sharma, S. (2017) ‘Non-rigid registration of multimodal images (Ultrasound and CT) of Liver using gradient orientation information’ in 2017 IEEE 2nd International Conference on Opto-Electronic Information Processing (ICOIP), IEEE, pp. 35-39.
3. Brandner, E.D., Wu, A., Chen, H., Heron, D., Kalnicki, S., Komanduri, K., Gerszten, K., Burton, S., Ahmed, I. and Shou, Z. (2006) Abdominal organ motion measured using 4D CT. International Journal of Radiation Oncology* Biology* Physics, Vol. 65 No. 2, pp.554-560.
4. Brendel, B., Rick, S.W.A., Stockheim, M. and Ermert, H. (2002) Registration of 3D CT and ultrasound datasets of the spine using bone structures. Computer Aided Surgery, Vol. 7 No. 3, pp.146-155.
5. Castro-Pareja, C.R., Zagrodsky, V., Bouchet, L. and Shekhar, R. (2005) Automated prostate localization in external-beam radiotherapy using mutual information-based registration of treatment planning CT and daily 3D ultrasound images in International Congress Series, Elsevier , Vol. 1281, pp. 435-440.

6. Collignon, A., Maes, F., Delaere, D., Vandermeulen, D., Suetens, P. and Marchal, G. (1995) Automated multi-modality image registration based on information theory in Information processing in medical imaging, Vol. 3, No. 6, pp. 263-274.

7. Crum, W.R., Hartkens, T. and Hill, D.L.G. (2004) Non-rigid image registration: theory and practice. The British journal of radiology, Vol. 77 Suppl. 2, pp.S140-S153.

8. Dhawan, A.P. (2012) Rigid and non-rigid medical image registration methods. International Journal of Biomedical Engineering and Technology, Vol. 8 No. 2-3, pp.200-219.

9. Haber, E. and Modersitzki, J. (2006) Intensity gradient based registration and fusion of multi-modal images in International Conference on Medical Image Computing and Computer-Assisted Intervention, Springer, Berlin, Heidelberg , pp. 726-733.

10. Huang, X., Li, H. and Zhu, Y. (2012) Hybrid deformable image registration using a closed-form Free Form Deformation approach. International Journal of Biomedical Engineering and Technology, Vol. 8 No.2-3, pp.245-258.

11. Hyun, D. G., Ra, J. B., Nam, W. H., Kang, D. G., & Lee, D. (2009) U.S. Patent Application No. 12/477,072.

12. Ino, F., Kawasaki, Y., Tashiro, T., Nakajima, Y., Sato, Y., Tamura, S. and Hagihara, K. (2005) 'A parallel implementation of 2-D/3-D image registration for computer-assisted surgery' in 11th International Conference on Parallel and Distributed Systems (ICPADS'05), Vol. 2, pp. 316-320, IEEE.

13. Kim, Y.S., Lee, J.H. and Ra, J.B. (2008) Multi-sensor image registration based on intensity and edge orientation information. Pattern recognition, Vol. 41 No. 11, pp.3356-3365.

14. Lange, T., Eulenstein, S., Hünerbein, M., Lamecker, H. and Schlag, P.M. (2004) Augmenting intraoperative 3D ultrasound with preoperative models for navigation in liver surgery in International Conference on Medical Image Computing and Computer-Assisted Intervention, Springer , Berlin, Heidelberg, pp. 534-541.

15. Lange, T., Papenberg, N., Heldmann, S., Modersitzki, J., Fischer, B., Lamecker, H. and Schlag, P.M. (2009) 3D ultrasound-CT registration of the liver using combined landmark-intensity information. International journal of computer assisted radiology and surgery, Vol. 4 No. 1, pp.79-88.

16. Lee, D., Nam, W.H., Lee, J.Y. and Ra, J.B. (2010) Non-rigid registration between 3D ultrasound and CT images of the liver based on intensity and gradient information. Physics in Medicine & Biology, Vol. 56 No. 1, p.117.

17. Lee, S., Wolberg, G. and Shin, S.Y. (1997) Scattered data interpolation with multilevel B-splines. IEEE transactions on visualization and computer graphics, Vol. 3 No. 3, pp.228-244.

18. Loucif, M. and Tighuiouart, B. (2019) A combined hierarchical algorithm of mammograms registration using mutual information and a point based matching approach. International Journal of Biomedical Engineering and Technology, Vol. 29 No. 3, pp.293-307.

19. Lu, X., Suo, S., Liu, H. and Zhang, S. (2012) Three-dimensional multimodal image non-rigid registration and fusion in a high intensity focused ultrasound system. Computer Aided Surgery, Vol. 17 No. 1, pp.1-12.

20. McGahan, J.P., Ryu, J. and Fogata, M. (2004) Ultrasound probe pressure as a source of error in prostate localization for external beam radiotherapy. International Journal of Radiation Oncology* Biology* Physics, Vol. 60 No. 3, pp.788-793.

21. Nam, W.H., Kang, D.G., Lee, D., Lee, J.Y. and Ra, J.B. (2011) Automatic registration between 3D intra-operative ultrasound and pre-operative CT images of the liver based on robust edge matching. Physics in Medicine & Biology, Vol. 57 No. 1, p.69.

22. Nocedal, J. (1980) Updating quasi-Newton matrices with limited storage. Mathematics of computation, Vol. 35 No. 151, pp.773-782.

23. Nocedal, J. and Wright, S. (2006) Numerical Optimization, Springer Science & Business Media, New York..

24. Penney, G. P. (2010) Applications in image guided interventions in IEEE ISBI Tutorial Notes, Tutorial on Biomedical Image Registration. IEEE.

25. Penney, G.P., Blackall, J.M., Hamady, M.S., Sabharwal, T., Adam, A. and Hawkes, D.J. (2004) Registration of freehand 3D ultrasound and magnetic resonance liver images. Medical image analysis, Vol. 8 No. 1, pp.81-91.

26. Penney, G.P., Blackall, J.M., Hayashi, D., Sabharwal, T., Adam, A. and Hawkes, D.J. (2001) Overview of an ultrasound to CT or MR registration system for use in thermal ablation of liver metastases in Proceedings of Medical Image Understanding and Analysis Vol. 1, pp. 6568.

27. Roche, A., Pennec, X., Malandain, G. and Ayache, N. (2001) Rigid registration of 3-D ultrasound with MR images: a new approach combining intensity and gradient information. IEEE transactions on medical imaging, Vol. 20 No. 10, pp.1038-1049.

28. Rohlfing, T., Maurer, C.R., O'dell, W.G. and Zhong, J. (2004) Modeling liver motion and deformation during the respiratory cycle using intensity-based nonrigid registration of gated MR images. Medical physics, Vol. 31 No. 3, pp.427-432.

29. Rueckert, D., Sonoda, L.I., Hayes, C., Hill, D.L., Leach, M.O. and Hawkes, D.J. (1999) Nonrigid registration using free-form deformations: application to breast MR images. IEEE transactions on medical imaging, Vol. 18 No. 8, pp.712-721.

30. Sederberg, T.W. and Parry, S.R. (1986) Free-form deformation of solid geometric models. ACM SIGGRAPH computer graphics, Vol 20 No. 4, pp.151-160.

31. Shimizu, S., Shirato, H., Xo, B., Kagei, K., Nishioka, T., Hashimoto, S., Tsuchiya, K., Aoyama, H. and Miyasaka, K. (1999) Three-dimensional movement of a liver tumor detected by high-speed magnetic resonance imaging. Radiotherapy and oncology, Vol. 50 No. 3, pp.367-370.

32. Studholme, C., Hill, D.L. and Hawkes, D.J. (1999) An overlap invariant entropy measure of 3D medical image alignment. Pattern recognition, Vol. 32 No. 1, pp.71-86.

33. Treece, G.M., Prager, R.W., Gee, A.H. and Berman, L (2002) Correction of probe pressure artifacts in freehand 3D ultrasound. Medical Image Analysis, Vol. 6 No. 3, pp.199-214.

34. Wein, W., Brunke, S., Khamene, A., Callstrom, M.R. and Navab, N. (2008) Automatic CT-ultrasound registration for diagnostic imaging and image-guided intervention. Medical image analysis, Vol. 12 No. 5, pp.577-585.

35. Wein, W., Kutter, O., Aichert, A., Zikic, D., Kamen, A. and Navab, N. (2010) Automatic non-linear mapping of pre-procedure CT volumes to 3D ultrasound in 2010 IEEE International Symposium on Biomedical Imaging: From Nano to Macro, IEEE, pp. 1225-1228.

36. Weon, C.J., Nam, W.H., Kim, J.B., Hwang, Y., Bang, W.C. and Ra, J.B. (2013) Robust feature based preregistration of 3D MR image to 3D B-mode ultrasound image of the liver in Proceedings of International Society of Magnetic Resonance in Medicine.

37. Weon, C.J., Nam, W.H., Lee, D., Hwang, Y., Kim, J.B., Bang, W.C. and Ra, J.B. (2012) Position estimation of moving liver lesion based on registration between 2D ultrasound and 4D MR images in 19th IEEE International Conference on Image Processing, IEEE, pp. 1677-1680.

38. Xie, Z. and Farin, G. (2001) 'Deformation with hierarchical B-splines', Mathematical Methods for Curves and Surfaces: Oslo 2000, Vanderbilt University Press, Nashville, pp.545–554.

39. Zhang, W., Noble, J.A. and Brady, J.M. (2006) Real time 3-D ultrasound to MR cardiovascular image registration using a phase-based approach in 3rd IEEE International Symposium on Biomedical Imaging: Nano to Macro, IEEE, pp. 666-669.